Pergamon

Ocean Engineering 28 (2001) 1171–1198

OCEAN ENGINEERING

Anomalous amplifications of semidiurnal tides along the western coast of Taiwan

Ming-Chung Lin [a], Wen-Jye Juang [a, b,*], Ting-Kuei Tsay [c]

[a] *Department of Naval Architecture and Ocean Engineering, National Taiwan University, Taipei 106, Taiwan*

[b] *Institute of Harbor and Marine Technology, Wu-chi 435, Taiwan*

[c] *Department of Civil Engineering, National Taiwan University, Taipei 106, Taiwan*

Received 30 January 2000; received in revised form 30 April 2000; accepted 24 May 2000

Abstract

By compiling all the tidal data gathered from island-wide results of simple harmonic analysis, anomalous amplifications of semidiurnal tides along the western coast of Taiwan are illustrated. The mechanisms are investigated both theoretically and numerically by applying the linear shallow-water wave equations. Waves trapped by a continental shelf and resonance of tidal co-oscillation are identified theoretically. Numerically, a two-dimensional finite element model is applied to real topography for tidal computations. The co-range and equi-phase charts of three main semidiurnal constituents (M_2, S_2, and N_2) and one diurnal constituent K_1 are calculated. Anomalous amplifications of semidiurnal tides that appear as partially standing waves are demonstrated. © 2001 Elsevier Science Ltd. All rights reserved.

Keywords: Semidiurnal tides; Continental shelf; Resonance; Trapped wave; Shallow water; Taiwan Strait; Finite element model

1. Introduction

Taiwan, also known as Formosa as shown in Fig. 1, is a spindle-shaped island surrounded by the East China Sea to the north, the Western Pacific Ocean to the east, the Bashi Channel and the South China Sea to the south, and the Taiwan Strait

* Corresponding author address: No. 2, Chung-Heng 10th Rd., Wu-Chi, Taichung 435, Taiwan. Fax: +886-4-657-1329.

E-mail addresses: dindong@linux.na.ntu.edu.tw (M.-C. Lin), wjjuang@ms1.hinet.net (W.-J. Juang), tktsay@ccms.ntu.edu.tw (T.-K. Tsay).

0029-8018/01/$ - see front matter © 2001 Elsevier Science Ltd. All rights reserved.
PII: S0029-8018(00)00049-4

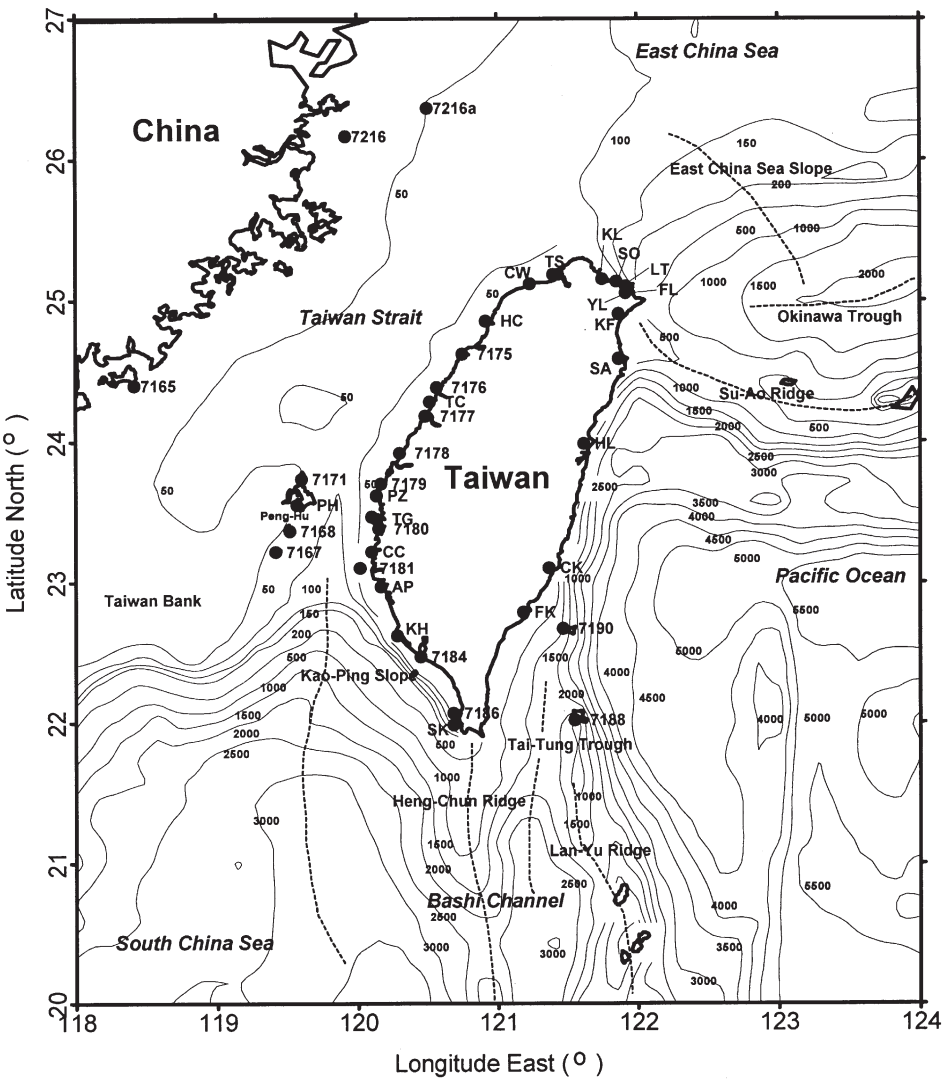

Fig. 1. Topography and tidal stations around Taiwan. Numbers show water depth in meters. Dotted lines represent the position of shelf slope, ridges, and troughs. Solid circles denote the tidal stations established by the Central Weather Bureau, Taiwan, and are represented by location abbreviation; stations reported in the Admiralty Tide Tables are represented by a bold number.

to the west. Topographically, the eastern coast of Taiwan just situates on the edge of the continental shelf of Asia. Out of the edge, submarine slopes plunge down to the Pacific Ocean at a grade of 1:10 and the ocean reaches a depth of more than 5000 meters about 50 kilometers off the coast. Along the northeastern and southwestern rims of the shelf edges, respectively, there can be located, the East China Sea Slope and the Kao–Ping Slope. Between these two slopes, the Okinawa Trough, the

Su–Ao Ridge, the Lan–Yu Ridge, the Tai–Tung Trough, and the Heng–Chun Ridge are staggered in a clockwise direction. The western coast is located in the Taiwan Strait, where the average depth is less than 80 meters, and is connected to the East China Sea and the South China Sea. In addition, there is the Taiwan Bank with most of the water depth less than 30 meters situated very close to the southward rim. The complexities of topography around Taiwan have been thought to have significant influences on tidal characteristics along the western coasts.

The mild-slope equation, a two-dimensional linear depth-integrated wave equation in the absence of the Coriolis force, can be applied to determine the motion of monochromatic waves propagating in a basin with moderate bottom slope (Berkhoff, 1972; Smith and Sprinks, 1975; Berkhoff et al., 1982). The significance of this equation is its applicability to a broad range of wave frequencies (Mei, 1983; Tsay, 1991). Moreover, Booij (1983) has shown that acceptable results can be achieved even though the bottom slope is not moderate. Kirby (1986) has extended the mild-slope equation to account for a fast-varying topography. By introducing the horizontal pseudo fluxes, Copeland (1985) has shown that the mild-slope equation can be transformed into forms similar to the shallow-water wave equations. Madsen and Larsen (1987) then developed an efficient ADI finite-difference algorithm to find the stationary solution by which large model areas can be handled with a relatively small amount of computational effort. However, numerical models of the mild-slope equation were scarcely employed in tidal computations.

For long waves incident normally or obliquely to an island, a stepped ridge or a shelf with two edges apart with a finite distance, phenomena of wave refraction, transmission, reflection as well as the scattering will occur. Mei (1983) has shown that certain sinusoidal waves may exist at a depth discontinuity, such as a ridge, but are unable to propagate from shallow to deep water. For this kind of trapped wave, there exist certain characteristic frequencies (or eigenfrequencies), corresponding to free oscillation modes. These modes can be important to resonate the Helmholtz modes in a basin with particular geometry (Snodgrass et al., 1962; Mysak, 1967; Miles, 1972; Meyer, 1979; Mei, 1983). On the other hand, Louguet-Higgins (1967, 1968, and 1969) had pointed out that waves could be trapped around a sufficiently large circular island by bottom topography. He also predicted that a trapped wave with certain frequencies could still remain in phase with itself after propagating one complete round. These trapped wave mechanisms can also occur in the sea surrounding Taiwan.

Co-oscillation is a kind of forced oscillation of which the characteristic frequency is the same as that of exciting sources. For a long wave propagating from the deep ocean into a channel of finite constant depth with a reflecting wall at one end, a resonant response to a co-oscillating tide can occur (Dean and Dalrymple, 1984).

Tides on the rotating earth, the attributes of large-scale motion measured by the Rossby number ($\varepsilon=U/2\Omega L$, where U is the horizontal characteristic velocity; L, the characteristic length; and $\Omega=7.3\times10^{-5}$ s^{-1}, the rotating angular frequency of the earth) will generally deviate from wave motions without rotation, as ε approaches to order one. This implies that the Coriolis effects are prominent and need to be considered in tidal hydrodynamics for large areas. Once the Coriolis effects are

included, a host of subtle and fascinating dynamic phenomena are possible (Pedlosky, 1979). However, for the size of a small sea surrounding Taiwan, Coriolis force may not be very important. In a study of tides in the Gulf of Thailand, Yanagi and Takao (1998a) found that the tidal periods of semidiurnal and diurnal constituents are much shorter than the inertia period ($T_i=2\pi/f$, where $f=2\Omega\sin\phi$, the Coriolis parameter; and ϕ, the latitude). The width of the gulf is also narrower than that of the Rossby deformation length ($\lambda=c/f$; $c=\sqrt{gh}$, the phase speed of long waves in water depth h). Therefore, they suggested that the Coriolis force in the Gulf of Thailand did not seriously affect the tidal phenomena.

During the past few decades, most of the local researchers inferred that the anomalous amplifications of tides along the western coast of Taiwan were mainly induced by encountering effects of tides, which generated in the West Pacific Ocean and diffracted from southern and northern ends of the island. Investigations on mechanisms of the amplification, however, are still lacking. In this paper, tidal constituents around Taiwan will be described first in the following section. In Section 3, reformulation of linear shallow-water wave equations to a form of the mild-slope equation is included. In this section, ignoring effects of Coriolis force for semidiurnal computations of tides around Taiwan is justified. In Section 4, to investigate possible mechanisms of the anomalous amplification of semidiurnal tides, the shallow-water wave theories mentioned earlier are applied to an idealized shelf of which the depth configuration is extracted from the topography around the coasts of Taiwan. In Section 5, to entirely take the topographic effects such as the continental shelf, bank, troughs, ridges, and islands into account, a finite element model (Tsay et al., 1989) is employed to solve the mild-slope equation. Finally, based on the computed co-range and equi-phase charts of semidiurnal tidal constituents, anomalous amplification mechanism of tides in the Taiwan Strait is examined. Comparisons between computational results and measured data with discussions are given in Section 6. Conclusions are summarized in the last section.

2. Tidal constituents analyses and topographical investigations

There are more than twenty tidal stations, as shown in Fig. 1, distributed around the coasts of Taiwan. Most of the tidal stations are established for long-term measurements to supplement engineering applications. By compiling all the harmonic analysis results gathered around the Taiwan's coasts, the amplitudes and phase-lags of main diurnal (P_1, O_1, K_1) and semi-diurnal (M_2, S_2, N_2) constituents at tidal stations are listed in Table 1. Let A_{O_1}, A_{K_1}, A_{M_2} and A_{S_2} represent the constituent amplitudes of O_1, K_1, M_2, and S_2, respectively, and use the identification criterion of tidal type (Hicks, 1989; Yanagi and Takao, 1998b),

$$F=\frac{A_{O_1}+A_{K_1}}{A_{M_2}+A_{S_2}}, \tag{1}$$

the diurnal type is defined as $F>1.25$, the semidiurnal type as $F<0.25$ and the mixed

Table 1
Amplitudes, H(m), and phase-lags, $g°$, of main tidal constituents compiled at tidal stations around Taiwan

No.	Place or station	Lat. N D°M′	Long. E D°M′	Harmonic constants											
				M_2		S_2		N_2		K_1		O_1		P_1	
				$g°$	H(m)	$g°$	H(m)	$g°$	H(m)	$g°$	H(m)	$g°$	H(m)	$g°$	H(m)
SA	Su-Ao Kang	24°35′	121°52′	169	0.418	201	0.181	158	0.082	226	0.197	191	0.171	223	0.065
KF	Geng-Fang	24°54′	121°52′	187	0.364	215	0.148	178	0.077	220	0.194	187	0.160	218	0.061
YL	Yan-Liao	25°03′	121°55′	198	0.206	216	0.106	190	0.051	220	0.191	187	0.157	216	0.062
LT	Long-Dong	25°06′	121°55′	209	0.225	230	0.113	198	0.056	222	0.199	188	0.165	218	0.066
SO	Shen-Ao	25°08′	121°51′	251	0.175	246	0.069	224	0.048	225	0.190	191	0.158	222	0.063
KL	Kee-Lung	25°09′	121°45′	278	0.219	281	0.056	246	0.056	228	0.187	194	0.156	225	0.062
TS	Tan-Shui	25°11′	121°24′	313	1.03	351	0.289	286	0.192	244	0.217	208	0.183	241	0.069
CW	Chu-Wei	25°07′	121°14′	316	1.196	355	0.341	289	0.221	248	0.224	211	0.189	244	0.069
HC	Hsin-Chu	24°51′	120°55′	319	1.610	360	0.467	293	0.291	257	0.235	218	0.199	253	0.073
TC	Tai-Chung	24°17′	120°31′	324	1.719	369	0.486	299	0.296	268	0.252	229	0.206	265	0.087
TH	Po-Zi-Liao	23°37′	120°08′	318	1.051	364	0.277	285	0.186	282	0.230	230	0.202	284	0.061
PH	Peng-Hu	23°33′	119°34′	324	0.892	373	0.223	298	0.163	280	0.249	237	0.216	275	0.081
WN	Wen-Kang	23°28′	120°06′	310	0.693	354	0.163	286	0.128	282	0.217	239	0.191	280	0.065
TG	Dong-Shi	23°27′	120°08′	314	0.654	360	0.15	288	0.120	285	0.208	243	0.182	281	0.062
CC	Chiang-Chun	23°13′	120°06′	313	0.463	351	0.098	282	0.077	287	0.187	244	0.161	286	0.059
AP	An-Ping	22°58′	120°10′	258	0.236	268	0.059	238	0.052	277	0.181	234	0.165	268	0.059
KH	Kao-Hsiung	22°37′	120°17′	218	0.169	223	0.066	193	0.043	283	0.162	234	0.154	279	0.062
SK	Xun-Guang-Zui	21°59′	120°41′	194	0.206	216	0.089	181	0.042	277	0.222	236	0.188	273	0.068
FK	Fu-Kang	22°47′	121°11′	172	0.430	203	0.170	161	0.075	231	0.167	196	0.161	224	0.051
CK	Cheng-Kuang	23°05′	121°22′	175	0.426	203	0.200	157	0.095	221	0.172	190	0.150	218	0.057
HL	Hua-Lian	23°59′	121°37′	175	0.426	204	0.192	154	0.079	220	0.147	195	0.137	213	0.049

type as $1.25 \geq F \geq 0.25$. One can see that semidiurnal tides dominate at most western coast stations, whereas stations SA (Su–Ao), KL (Kee–Lung), AP (An–Ping), and KH (Kao–Hsiung) are diurnal tide dominant. This indicates that the tides changed their characteristics after propagating onto the continental shelf (see Fig. 1).

To gain more insight into the anomalous amplification of tides, one can plot tidal amplitudes and phase-lags of all stations around Taiwan, Fig. 2(a). As can be seen, the amplitudes of diurnal constituents P_1, O_1, and K_1 remain almost constant for all stations even at station TC (Tai–Chung) which has the highest semidiurnal amplitudes. In other words, amplifications of diurnal constituents are not conspicuous around the coasts of Taiwan. However, amplifications of semidiurnal constituents are more prominent along the western coast. For M_2, S_2, and N_2 constituents, respectively, the amplitudes at northeastern station SO (Shen–Ao) are 0.175 m, 0.069 m, and 0.048 m; at central western station TC are 1.719 m, 0.486 m, and 0.296 m; and at southwestern station KH are 0.169 m, 0.066 m and 0.043 m. Evidently, the amplification factors of station TC relative to station SO are 9.82 for M_2, 7.04 for S_2, and 6.17 for N_2, while the amplification factors of station TC relative to station KH are 10.17 for M_2, 7.36 for S_2, and 6.88 for N_2.

Physically, the difference of phase-lag can be used to indicate the time that tides take to propagate from one station to another. From Fig. 2(b), the phase-lag difference of diurnal constituents between station SA on the northeastern coast and station CC (Chiang–Chun) on the southwestern coast is about 45 degrees. Equivalently, it takes about three hours for diurnal tides to propagate from the northeastern to the southwestern coast. For semidiurnal tides, differences of phase-lag between central western coast station TC and station SA is about 150 degrees. It takes approximately five hours for semidiurnal tides to propagate between these two stations. In addition, along the northern coast from station SA to station TS (Tan–Shui), it takes four hours for semidiurnal tides to travel a distance of less than 100 km. However, the same time is needed along the southern coast from station SK (Xun–Guang–Zui), the southernmost station of Taiwan, to station CC with a distance longer than 200 km.

To consider the effects of topography, a typical profile of water depth, starting from eastern station CK (Cheng–Kung) in the counterclockwise direction, with a distance of 50 km off the coast around the island is shown in Fig. 3. Excluding the ridges and troughs, it is interesting to note that there is a shelf-like topography with the length of about 650 km, extending from station LT (Long–Dong) on the northeastern coast to AP on the southwestern coast. It is observed that station SO, having the smallest semidiurnal amplitudes on the northeastern coast, is situated near the edge of the shelf. The station KH, is located right outside of the shelf on the slope and also has the minimal semidiurnal amplitudes on the southwestern coast. Moreover, the station TC with the highest semidiurnal amplitudes on the central western coast is roughly at the middle of the shelf.

3. The shallow-water wave equations

In this section, model equations with effects of topography and Coriolis effects will be discussed. A region surrounding Taiwan spans only approximately seven

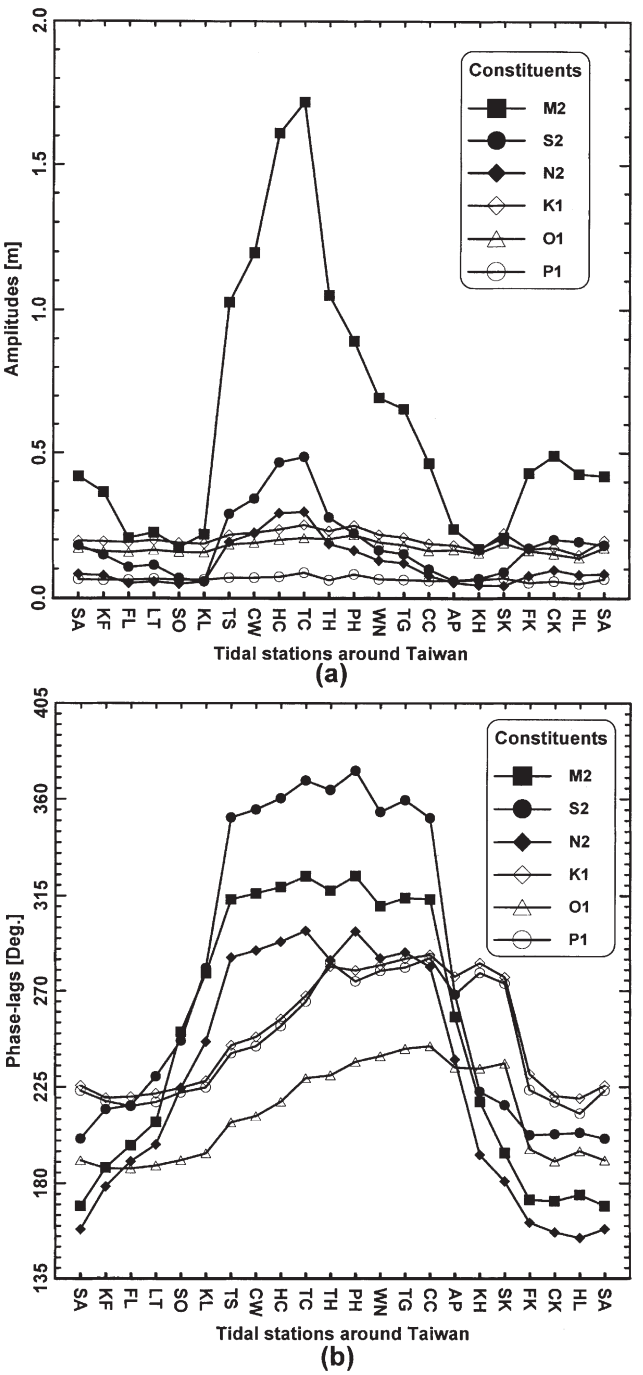

Fig. 2. Distribution of amplitudes, (a) and phase-lags, (b) of measured tidal constituents around Taiwan.

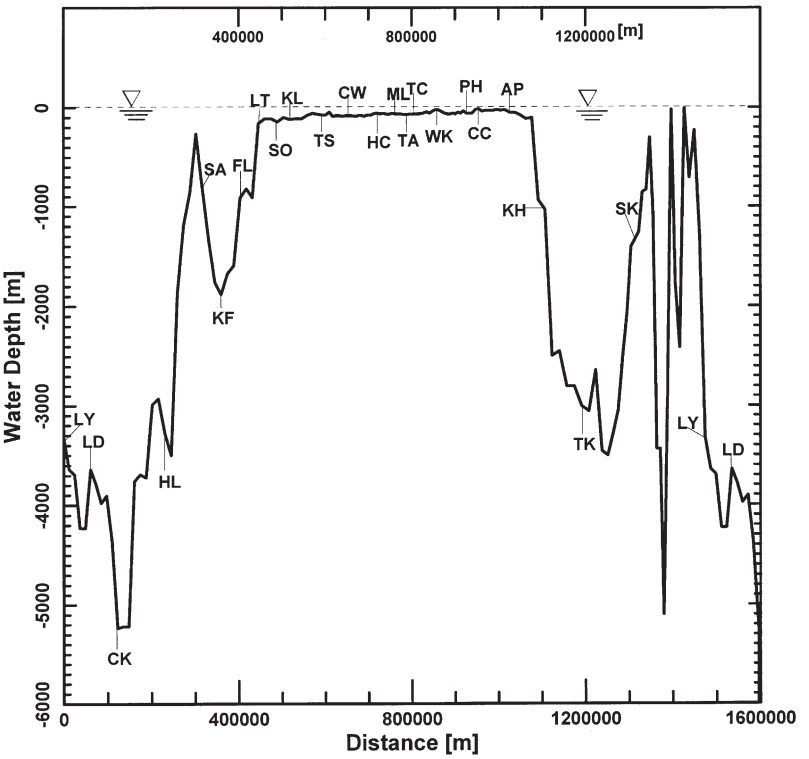

Fig. 3. Typical topographic profile (a shelf) at a distance of 50 km off the coast around Taiwan.

degrees in latitude (Fig. 1). Therefore, the Coriolis parameter, f, can be assumed constant. Assuming that the vertical variation is weak and the vertical acceleration is small compared with gravitational acceleration, g, and free surface displacement, ξ, is small compared to undisturbed water depth $h(x,y)$, the linearized shallow-water wave equations are written as

$$\frac{\partial U}{\partial t}+f\vec{\mathrm{e}}\times U=-g\nabla\xi \tag{2}$$

$$\frac{\partial \xi}{\partial t}+\nabla\cdot(hU)=0, \tag{3}$$

where $\nabla=(\partial/\partial x,\partial/\partial y)$ denotes the space gradient operator on the horizontal right-hand Cartesian coordinate (x,y), t the time, $\vec{\mathrm{e}}$ the vertical unit vector following the right-hand rule, $U(x,y,t)$ the depth-averaged velocity vector. Without losing the generality in treating the linear problems of tidal constituents, harmonic assumption in time t can be made. Hence,

$$(U,\xi)=(u,\zeta)e^{i\sigma t}, \tag{4}$$

where $u=(u,v)$ denotes the amplitude of the depth-averaged velocity components in x and y directions, ζ the amplitude of free surface displacement, and σ the characteristic frequency of certain constituent. Eqs. (2) and (3) then can be combined into

$$\nabla^2\zeta+\frac{1}{h}(\nabla\zeta\cdot\nabla h)-i\frac{f}{h\sigma}\vec{e}\cdot(\nabla\zeta\times\nabla h)+\frac{\sigma^2-f^2}{gh}\zeta=0. \tag{5}$$

Incorporating the impermeable bottom boundary condition into Eq. (5), the shallow-water wave equation then can be reduced straightforwardly to the form similar to the Helmholtz equation (Chambers, 1965; Louguet-Higgins 1968, 1969; Mysak and Tang, 1974):

$$\nabla^2\zeta+\frac{\sigma^2-f^2}{gh}\zeta=0 \tag{6}$$

where ∇^2 denotes the two-dimensional Laplacian operator $(\partial^2/\partial x^2+\partial^2/\partial y^2)$. Utilizing the hypothesis of $|\nabla h|=O(h/L)\ll 1$, where L denotes the characteristic wavelength, Eq. (6) can then be reformulated as the mild-slope equation (Berkhoff, 1972; Smith and Sprinks, 1975; Booij, 1983; Kirby, 1986; Tsay, 1991) such that the variation of h can be incorporated:

$$\nabla\cdot(gh\nabla\zeta)+(\sigma^2-f^2)\zeta=0 \tag{7}$$

One may take the predominant semidiurnal constituent M_2 on a shelf around the coasts of Taiwan to evaluate the importance of the f^2 term. Due to the characteristic period of M_2 of 12.4206 hrs, the characteristic latitude of Taiwan $\theta=25°$N, the value of $f^2/\sigma^2\approx 1/5$. Therefore, $\sigma^2>>f^2$ could be a reasonable assumption for problems associated with semidiurnal tides in low latitude seas. Hence, the Coriolis effects are ignored in the following discussions.

4. Theoretical analysis

Many researchers (Louguet-Higgins 1967, 1968; Mei, 1983; Dean and Dalrymple, 1984) have studied the importance of bottom topography on behaviors of surface water waves. Based on Eq. (7) after neglecting the Coriollis effects, some simple cases of long waves propagating over a continental shelf are considered in this section.

Let the continental shelf shown in Fig. 3 be idealized as a shelf with a stepwise variation of depth as shown in Fig. 4(a). Adapting the analysis that Mei (1983) used to investigate waves scattered by a shelf or trough of finite length, the general solution over each constant-depth region for an obliquely incident long wave with unit amplitude arrives from the north ($x\sim+\infty$) can be written as:

$$\zeta_1=e^{i\beta y}(e^{i\alpha_1(x-a)}+R'e^{i\alpha_1(x-a)}),\alpha_1^2+\beta^2=k_1^2(=\sigma^2/gh_1),x>a, \tag{8}$$

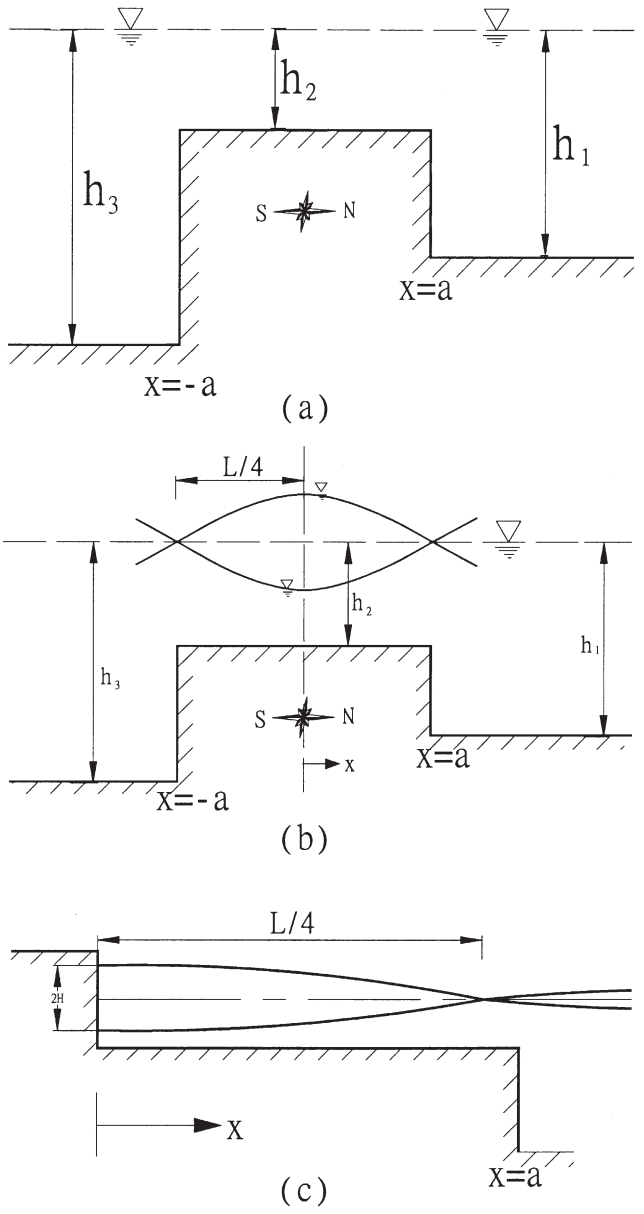

Fig. 4. Definition of an idealized topographic shelf, (a); with partially standing waves, (b); and with co-oscillating tides, (c).

$$\zeta_2 = e^{i\beta y}(Ae^{i\alpha_2 x} + Be^{i\alpha_2 x}), \alpha_2^2 + \beta^2 = k_2^2 (= \sigma^2/gh_2), -a < x < a, \tag{9}$$

$$\zeta_3 = T' e^{i\beta y} e^{i\alpha_3 (x-a)}, \alpha_3^2 + \beta^2 = k_3^2 (= \sigma^2/gh_3), x < -a. \tag{10}$$

where σ is the incident wave frequency, a_i; i=1, 2, and 3, and β are components of the wave number in x- and y-directions, respectively. h_i and k_i; i=1, 2, and 3, are water depth and wave number in different shelf regions. R', A, B, and T' are the corresponding wave amplitudes. $2a$ denotes the shelf length. Defining $R = R' e^{-2i\alpha_1 a}$ as the reflection coefficient, $T = T' e^{-i(\alpha_1 + \alpha_2)a}$ as the transmission coefficient, and applying the matching conditions: ζ and $h\partial\zeta/\partial x$ are continuous at the depth discontinuities, $x = \pm a$, of the shelf edges, the amplitudes A, B, R', and T' then can be solved, respectively, as:

$$A = \frac{1}{2} T' e^{-i\alpha_2 a}(1 + S_{32}), \tag{11}$$

$$B = \frac{1}{2} T' e^{i\alpha_2 a}(1 - S_{32}), \tag{12}$$

$$R' = \frac{e^{2i\alpha_2 a}[-(1 - S_{12})(1 + S_{32}) + (1 + S_{12})(1 - S_{32})e^{2i\alpha_2 a}]}{\Delta}, \tag{13}$$

$$T' = \frac{4S_{12}}{\Delta}, \tag{14}$$

where $S_{ij} = \alpha_i h_i / \alpha_j h_j$ is the ratio of relative water depth between regions i and j (no summation) with i,j=1, 2, and 3, respectively;

$$\Delta = (1 + S_{12})(1 + S_{32})e^{-2i\alpha_2 a} - (1 - S_{12})(1 - S_{32})e^{2i\alpha_2 a}. \tag{15}$$

The free surface on the shelf is obtained as:

$$\zeta_2 = e^{i\beta y}\left[\frac{2S_{12}(1 + S_{32})}{\Delta} e^{i\alpha_2 (x+a)} + \frac{2S_{12}(1 - S_{32})}{\Delta} e^{i\alpha_2 (x+a)}\right]. \tag{16}$$

For a symmetric shelf with water depth $h_1 = h_3$, it follows that $\alpha_1 = \alpha_3$,

$$S_{12} = S_{32} = \frac{\alpha_1 h_1}{\alpha_2 h_2} \equiv S = \frac{h_1}{h_2}\left(\frac{\sigma^2/gh_1 - \beta^2}{\sigma^2/gh_2 - \beta^2}\right)^{1/2} > 1. \tag{17}$$

and Eq. (16) is reduced to

$$\zeta_2 = e^{i\beta y} \frac{2S[(1 + S)e^{-i\alpha_2 (x-a)} + (1 - S)e^{i\alpha_2 (x+a)}]}{(1 + S)^2 e^{-2i\alpha_2 a} - (1 - S)^2 e^{2i\alpha_2 a}} \tag{18}$$

Obviously, the free surface displacement within $-a < x < a$ represents a partially standing wave with amplitude varying along x. The partially standing wave is com-

posed of two wavetrains traveling in opposite directions and is hence resulted in interference. Moreover, when $\sin^2 2\alpha_2 a=1$ or

$$2a=\frac{(2n-1)\pi}{2\alpha_2},\ n=1,2,3,\ldots \tag{19}$$

the interference at $x=-a$ is destructive, and the minimum transmission as well as the maximum reflection will be achieved (Mei, 1983). The corresponding values of transmission and reflection are

$$\min |T|^2=\frac{4S^2}{(1+S^2)^2}, \tag{20}$$

$$\max |T|^2=\frac{(1-S^2)^2}{(1+S^2)^2}. \tag{21}$$

When waves are normally incident to a shelf and one requires that the energy leak to infinity through transmission be minimized, the length of the shelf can be found as $2a=(2n-1)L/4$, where $n=1, 2, 3,\ldots, L$ denotes the wavelength over the shelf. However, from Eqs. (13) and (14), it is noted that wave transmission and reflection will always occur on a shelf.

For a shelf located behind a spindle-shaped island such as the western coast of Taiwan, effects of wave diffraction can be viewed as oscillation phenomena of two harmonic long waves normally reaching the shelf from both ends towards the central shelf. Assuming that the corresponding amplitudes at southern and northern ends, a_S and a_N, are small due to destructive interference, the long waves propagating from different directions are expressed as:

$$\zeta_S=a_S e^{-i(\sigma t+\theta_1)};\ a_S,\theta_1\in R, \tag{22}$$

$$\zeta_N=a_N e^{-i(\sigma t+\theta_2)};\ a_N,\theta_2\in R. \tag{23}$$

The free surface displacement on the shelf is expressed as:

$$\zeta=a_1 e^{i(kx-\sigma t+\theta_3)}+a_2 e^{i(-kx-\sigma t+\theta_4)},\ k=\sigma/\sqrt{gh_2}. \tag{24}$$

where θ_i; $i=1$, 2, 3, and 4, are phase-lags in different shelf regions. Applying the matching condition $\zeta_{x=-a}=\zeta_S$ and $\zeta_{x=a}=\zeta_N$ at $x=\pm a$, one has

$$a_1 e^{i(-ka+\theta_3)}+a_2 e^{i(ka+\theta_4)}=a_S e^{-i\theta_1}, \tag{25}$$

$$a_1 e^{i(ka+\theta_3)}+a_2 e^{i(-ka+\theta_4)}=a_N e^{-i\theta_2}. \tag{26}$$

The phase-lags, θ_3 and θ_4, and the amplitudes, a_1 and a_2, can be expressed in terms of θ_1, θ_2, a_S, and a_N:

$$\tan\theta_3=\frac{a_N\cos(ka-\theta_2)-a_S\cos(ka+\theta_1)}{a_N\sin(ka-\theta_2)+a_S\sin(ka+\theta_1)}, \tag{27}$$

$$\tan\theta_4=\frac{a_N\cos(ka-\theta_2)-a_S\cos(ka+\theta_1)}{a_N\sin(ka-\theta_2)+a_S\sin(ka+\theta_1)}, \tag{28}$$

$$a_1=\frac{a_N[\cos(ka-\theta_2)+\sin(ka-\theta_2)]-a_S[\cos(ka+\theta_1)-\sin(ka+\theta_1)]}{2\sin(2ka)(\cos\theta_3-\sin\theta_3)}, \tag{29}$$

$$a_2=\frac{a_N[\sin(ka-\theta_2)+\cos(ka-\theta_2)]-a_S[\sin(ka+\theta_1)-\cos(ka+\theta_1)]}{2\sin(2ka)(\cos\theta_4-\sin\theta_4)}. \tag{30}$$

Substituting Eqs. (29) and (30) into Eq. (24), for $\cos\theta_i\neq\sin\theta_i$; i=3 and 4, with the condition of $\sin 2ka=0$, one can obtain:

$$2a=nL/2,\ L\frac{2\pi}{\sigma}\sqrt{gh_2},\ n=1,2,3,\ldots \tag{31}$$

Evidently, the first resonance will occur when one half of the wavelength of partially standing waves on a shelf, as shown in Fig. 4(b), is equal to the shelf length, $2a$.

Due to interference such that partially standing waves will always appear on a shelf, a symmetric shelf, therefore, can be simplified with an impervious wall located right at the middle of the shelf length (x=0) as shown in Fig. 4(c). When a long wave with amplitude $H/2$ reaches such a shelf, the free surface displacement, ζ, on the shelf can be expressed straightforwardly by superposing the incident wave, ζ_i and the reflected wave, ζ_r, so a purely standing wave system can be formed and written as:

$$\zeta\equiv\zeta_i+\zeta_r=\frac{H}{2}\cos(kx-\sigma t)+\frac{H}{2}\cos(kx+\sigma t).\ =H\cos\sigma t\cos kx \tag{32}$$

Following the analyses of Dean and Dalrymple (1984), the distance from wall to the node (the position for which ζ=0) can be found by equating the spatial phase function of ζ to $\pi/2$, that is, $kx_{\text{node}}=\pi/2$, or

$$x_{\text{node}}=\frac{L}{4}, \tag{33}$$

and the range of the free surface displacement at the entrance to the shelf is

$$|\zeta_{x=a}|=H|\cos ka|. \tag{34}$$

The amplification factor of free surface displacement at the wall can be evaluated by relating $\zeta_{x=0}$ to $\zeta_{x=a}$:

$$\left|\frac{\zeta_{x=0}}{\zeta_{x=a}}\right|=\frac{1}{|\cos ka|}. \tag{35}$$

For a symmetric shelf with half of the length equaling $(2n-1)L/4$, $n=1, 2,\ldots$, the amplification factor in Eq. (35) approaches infinity. In other words, for a symmetric shelf with length $2a$, the co-oscillating resonance excited by a harmonic long wave with wavelength L will occur, when

$$2a=(2n-1)L/2,\ n=1,2,3,\ldots \tag{36}$$

When $n=1$, it is noted that the shelf length for co-oscillating resonance is exactly the same as that for partially standing waves as indicated in Eq. (31).

The phenomenon of semidiurnal amplification can also be investigated by examined theories of trapped waves. For waves trapped on a symmetrical shelf, the general form of free surface displacement still remains as Eq. (9). However, the solutions of trapped waves attenuated to zero at infinity on either side of the shelf (Mei, 1983) are:

$$\zeta_1=Ce^{i\beta y}e^{-\alpha_1(x-a)},\ x>a, \tag{37}$$

$$\zeta_3=De^{i\beta y}e^{\alpha_1(x+a)},\ x<-a, \tag{38}$$

where C and D are the corresponding wave amplitude, $\alpha_1=(\beta^2-k_1^2)^{1/2}$ and $K_2>\beta>k_1$, or

$$\beta(gh_1)^{1/2}>\sigma>\beta(gh_2)^{1/2}. \tag{39}$$

Applying the matching conditions of ζ and $h\partial\zeta/\partial x$ at both edges $x=\pm a$ of the shelf, a nontrivial condition for solving the amplitudes A, B, C, and D can be obtained as

$$(s-i)^2e^{-2i\alpha_2 a}-(s+i)^2e^{2i\alpha_2 a}=0, \tag{40}$$

where $s=\alpha_1h_1/\alpha_2h_2$.

Let~tan $\sigma=s$, σ then can be solved from Eq. (40) as:

$$\delta=\frac{1}{2}n\pi+\alpha_2 a,\ n=1,2,3,\ldots \tag{41}$$

In addition, by changing the variables

$$\chi=a(k_2^2-\beta^2)^{1/2}=\alpha_2 a, \tag{42}$$

Eq. (40) is transformed as:

$$\frac{(h_2/h_1)\chi}{(\chi_*^2-\chi^2)^{1/2}}=\begin{pmatrix}\cot\chi\\ -\tan\chi\end{pmatrix},\begin{pmatrix}n=\text{even}\\ n=\text{odd}\end{pmatrix}, \tag{43}$$

with

$$\chi_*^2=k_2^2a^2\left(1-\frac{h_2}{h_1}\right)=\frac{(\sigma a)^2}{gh_2}\left(1-\frac{h_2}{h_1}\right). \tag{44}$$

For a given wave frequency σ and shelf geometry χ_*, the parameter of χ as well as the eigenwavenumber, α_2, can be solved from Eqs. (43) and (42), respectively. To identify the appearances of trapped waves on a topographical shelf, the first three modes are shown in Fig. 5 (Mei, 1983) for references with present theoretical investigations.

Let the water depths of the topographical shelf that exists around the western coast of Taiwan be estimated for analyses with h_2=80 m on the shelf and h_1=h_3=5000 m on both sides. The total shelf length of $2a\cong$650 km is read directly from Fig. 3. Assume T=12.4206 hours (σ=1.405×10^{-4} s^{-1}) denotes the characteristic period (frequency) of semidiurnal tides (actually, it is the period of M_2), hence the phase velocity on the shelf C_2 ($=\sqrt{gh_2}$), wave numbers k_2 ($=\sigma/C_2$), and wavelength L_2($=2\pi/k_2$) are calculated to be 28 m/s, 5.018×10^{-6} m^{-1} and 1252 km, respectively. It is found that the wavelength of M_2 is very close to twice the shelf length.

Could trapped waves be the possible mechanism for the anomalous amplification of semidiurnal tides along the western coast of Taiwan? Using the values of h_i, i=1, 2, and 3, and $2a$ mentioned above and from Eqs. (43) and (44), one can determine $\chi_*\approx1.618\cong0.5\pi$. From graphical solution (see Fig. 6.1 of Mei, 1983) for $0<\chi_*<\pi$, there is only one even trapped mode occurring at $\chi\cong\pi/2$of which the displacement of free surface is proportional to cos$\alpha_2 x$ (Fig. 5). Substituting χ into Eq. (42) and letting $\alpha_2(=2_\chi/L_{2x}\approx k_2)$=4.83×10^{-6} m^{-1} with L_{2x}=4a denoting the distance two times of total length of the physical shelf, $\beta[=(k_2^2-\alpha_2^2)^{1/2}]$ can be calculated to be 1.36×10^{-6} m^{-1} and therefore satisfies the assumption $k_2>\beta>k_1$ [since $k_1(\sigma/\sqrt{gh_1})$=6.348×10^{-7} m^{-1}]. Subsequently, the theoretical length of the shelf can be estimated as

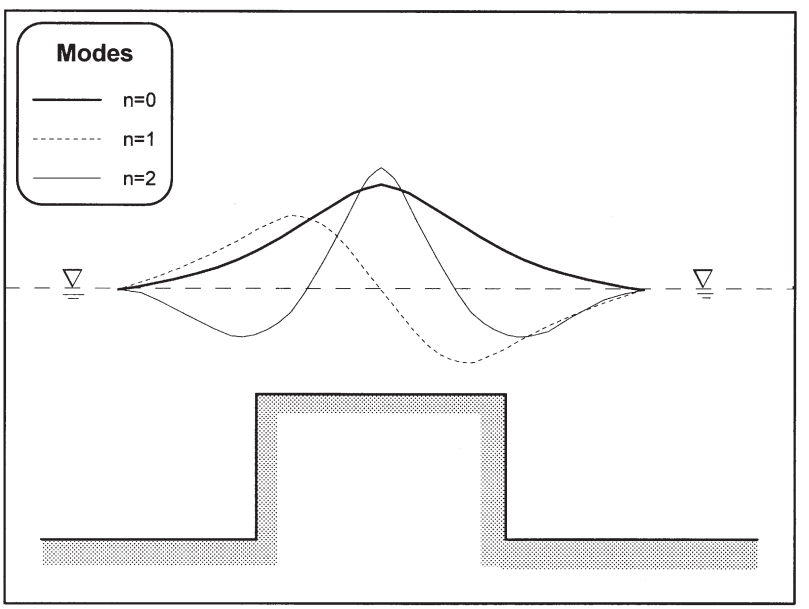

Fig. 5. The first three modes of waves trapped on a symmetric shelf (Mei, 1983).

$2a=2\chi/\alpha_2 \approx L_{2x}/2=650$ km. It is in good agreement with not only the geometrical length of physical shelf but also the pattern of free surface displacement appearing along the western coast of Taiwan. This indicates that the anomalous amplification of semidiurnal tides could be mainly induced by trapped waves. Furthermore, care must be taken with the form of standing waves. Eqs. (24) and (32) actually are very similar to that of waves trapped with even modes, of which the displacement of free surface is proportional to $\cos\alpha_2 x$. By setting $n=1$ in Eqs. (31) and (36), the resonant conditions resulted from partially standing waves and tidal co-oscillation, respectively, will be satisfied with the length of physical shelf approximate to $2a=L_2/2=626$ km. Therefore, more than one theory can be applied to explain the anomalous amplification of semidiurnal tides on the western coast of Taiwan.

5. A finite-element hydrodynamic model

To overcome the numerical difficulties arising from specifying open boundary conditions which are usually unknown except at a very few field stations, a two-dimensional mild-slope finite element wave model suitable for varying topography and compatible to Eq. (7) after neglecting the Coriollis effects is employed here (Tsay et al., 1989; Tsay, 1991). The model equation is

$$\nabla\cdot(PG\nabla\zeta)+k^2PG\zeta=0, \tag{45}$$

where P and G are phase and group velocity, respectively,

$$P=\frac{\sigma}{k}, \tag{46}$$

$$G=\frac{1}{2}\left(1+\frac{2kh}{\sinh 2kh}\right)P, \tag{47}$$

and k is a real number for propagating wave modes which satisfies the dispersion relationship,

$$\sigma^2=gk\tanh kh. \tag{48}$$

Eq. (45) reduces to the shallow-water wave equation, Eq. (7), for long waves. With the coordinate systems defined in Fig. 6, the incident wave in general can be expressed as

$$\zeta^I=A_0e^{ik_0r\cos(\theta-\theta^I)}, \tag{49}$$

where A_0 is amplitude, k_0 the incident wave number, θ^I the incident angle measured from the positive x axis in counterclockwise sense. The computational domain Θ around the main island of Taiwan is discretized with linear triangular isoparametric elements (Fig. 7), of which Γ_0 denotes the open-sea artificial boundary, Γ_{C_1} and Γ_{C_2} denotes the boundaries of physical coastlines. Applying the impermeable or zero-depth boundary conditions to the irregular coastlines Γ_{C_1} and Γ_{C_2}, one has:

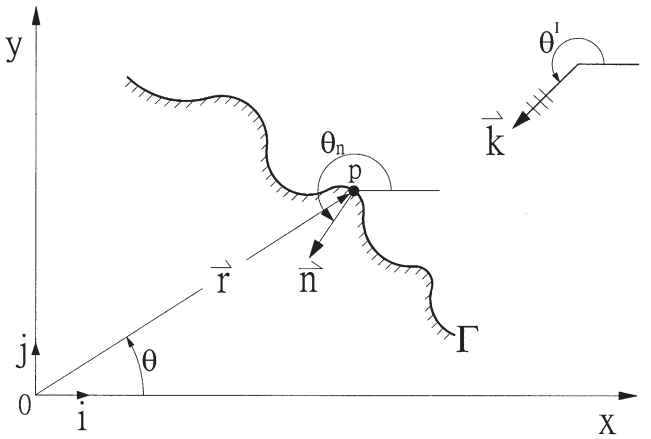

Fig. 6. Schematic definition of irregular coastlines and incident waves on the Cartesian and polar coordinate system.

$$PG\frac{\partial\zeta}{\partial n}=0. \tag{50}$$

The free surface displacement in the computational domain can be expressed by linear superposition:

$$\zeta=\zeta^I+\zeta^S, \tag{51}$$

where ζ^S represents the scattered waves (Chen and Mei, 1974) satisfying the radiation condition on open boundaries Γ_0:

$$\frac{\partial\zeta^S}{\partial n}-ik\zeta^S=0. \tag{52}$$

Since the depths along the open boundaries do not always pertain to constant, local wave number k in Eq. (52) thus must be implemented. It has been validated when the location of the open boundary is at least one and half times the incident wavelength away from the scatter (Chen and Tsay, 1990). Using the Galerkin Finite Elements Method (FEM), Eq. (45) then can be discretized as

$$\iint_{\Theta}[\nabla W\cdot(PG\nabla\zeta)-k^2PGW\zeta]dA-\int_{\Gamma_0}WPG[ik\zeta\cos(\theta_n-\theta)+\frac{1\partial\zeta}{r\partial\theta}\sin(\theta_n \tag{53}$$

$$-\theta)]dl=\int_{\Gamma_0}WPGi\cos(\theta_n-\theta)[k-k_0\cos(\theta-\theta^I)]\zeta^I dl,$$

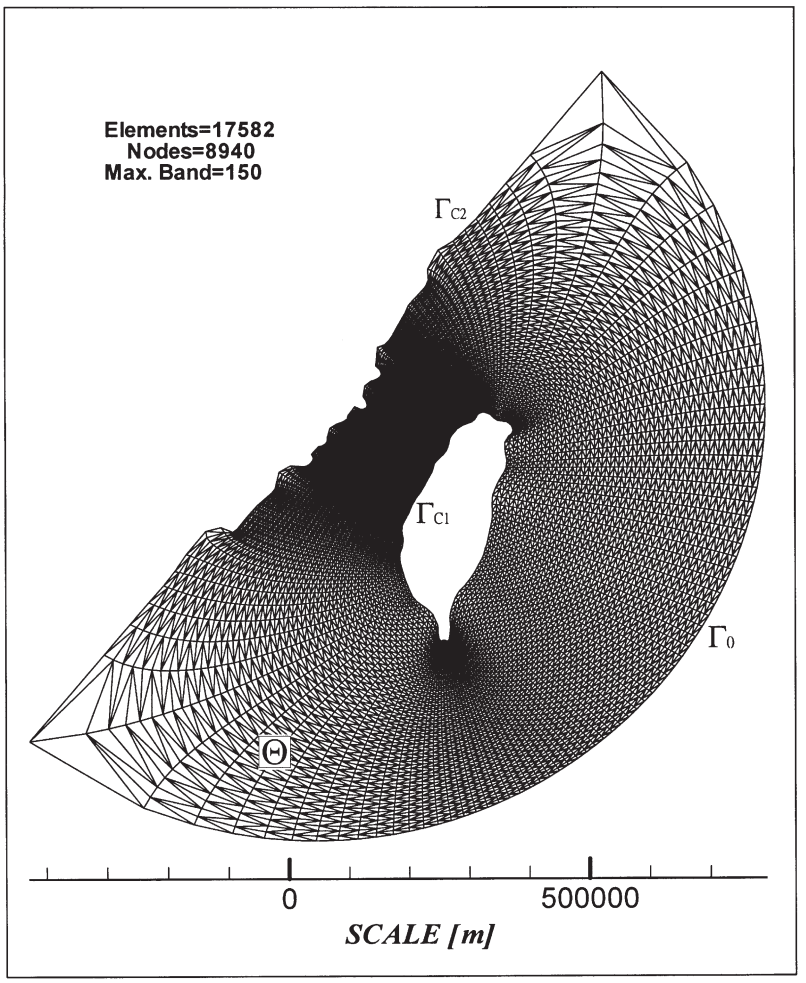

Fig. 7. Computational domain and its discretization with triangular isoparametric elements.

where W is the shape function. To solve the free surface displacement ζ as well as the phase angle in Eq. (53), only the incident angle, θ^I and amplitude, A_0 are needed and have to be calibrated in present numerical computations.

6. Numerical analysis

In tidal computations around Taiwan, the incident angle of specific tidal constituent is assumed between the South China Sea (θ^I=80°) and the Pacific Ocean (θ^I=210°). After incident angles of 80°, 120°, 180° and 210° are tested, it is found that the tidal waves with incident angle, θ^I, of 180° gives the best results, and they

are presented here. The amplitude of incident tides for numerical computations is assumed to be unity without losing the generality of the present linear model. Both the computed amplitudes and phase angles are calibrated according to that of the referenced station TC. The computed phase angles are then converted to phase-lags as used in harmonic analysis.

Compared with field data, the computed M_2 co-range associated with the equi-phase charts are shown in Figs. 8(a) and (b), respectively. From the computed co-range chart, one can easily see that a partially standing wave system exists on the western coast of Taiwan, one node of which is located at the northeastern coast near the Okinawa Trough. The other node is located at the southwestern coast near the Kao–Ping Slope. From the equi-phase chart, the phase difference between the station TC (the antinode) and either node is close to 90°. Moreover, the phase angle of M_2 increases monotonically from 0° to 360° around Taiwan in the clockwise direction and remains perfectly in phase with itself. Present results match the description that trapped waves always propagate around an island in a clockwise sense in the northern hemisphere (Louguet-Higgins, 1969).

Across a cross-section from Wuqiu–Yu, a reef islet near the eastern coast of China, to station TC, amplitude distribution of the partially standing waves looks very similar to that of Poincare waves, although the computation has neglected the Coriolis effects. The distribution of free-surface amplitudes, as shown in Fig. 9, clearly not only appears in a form of exponential decay from the eastern coast of China to the western coast of Taiwan but also shows the impervious boundary effects at both ends. Due to the bathymetry of the shelf being so flat both in longitudinal and latitudinal directions, the Poincare waves thus result in the free oscillation modes that could exist in a finite length channel, (Pedlosky, 1979), such as the Taiwan Strait.

Comparisons of amplitudes between field measurements and numerical results of M_2 constituent are shown in Fig. 10(a). Good agreements are observed not only along the western coast of Taiwan but also at a western offshore station Peng–Hu (PH), except those along the eastern stations from SA to SO and from SK to SA. It is worth pointing out that at the southwestern coast of Taiwan, the computed node of oscillation is located near station KH and is in good agreement with measured data. Nevertheless, the other node is found to be on the northeastern coast of Taiwan near station Fu–Lung (FL), compared to the measured one at station SO. The southward shift of nodal position from SO to FL in physical scale is not more than 20 km. Comparisons of phase-lags between measurements and computational results are shown in Fig. 10(b). Evidently, excellent agreements exist on most of the tidal stations except at the northern coast from stations FL to KL. It is noted that relatively significant discrepancy in both amplitude and phase angle occur at the northern coast of Taiwan. The phase difference between stations FL (a node) and TC (the antinode) is closer to 90° in field data than numerical results. These discrepancies might be a result of neglecting the Coriolis effects in the present study or the crude representation of topography.

In order to identify further anomalous amplification mechanisms of semidiurnal tides, two more numerical cases of S_2 and N_2 constituents are implemented and their co-range and equi-phase charts are shown in Figs. 11 and 12, respectively. From the

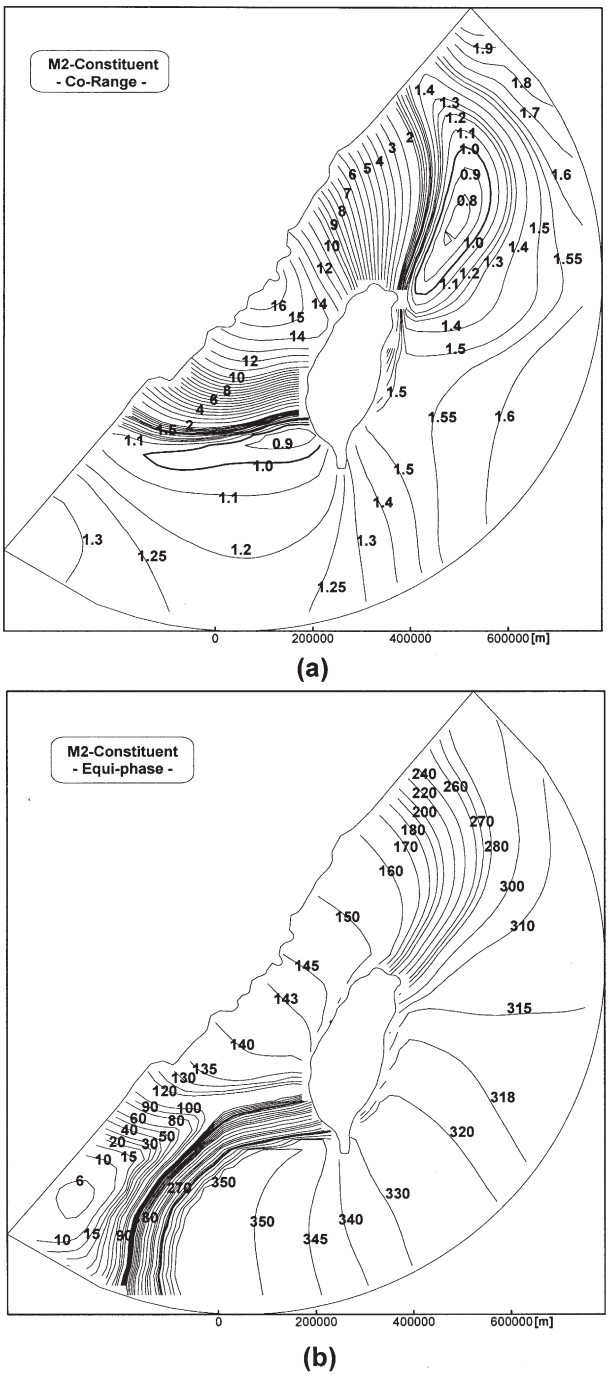

Fig. 8. Numerical co-range (a); and equi-phase (b) charts of the M_2 constituent with incident angle of 180°.

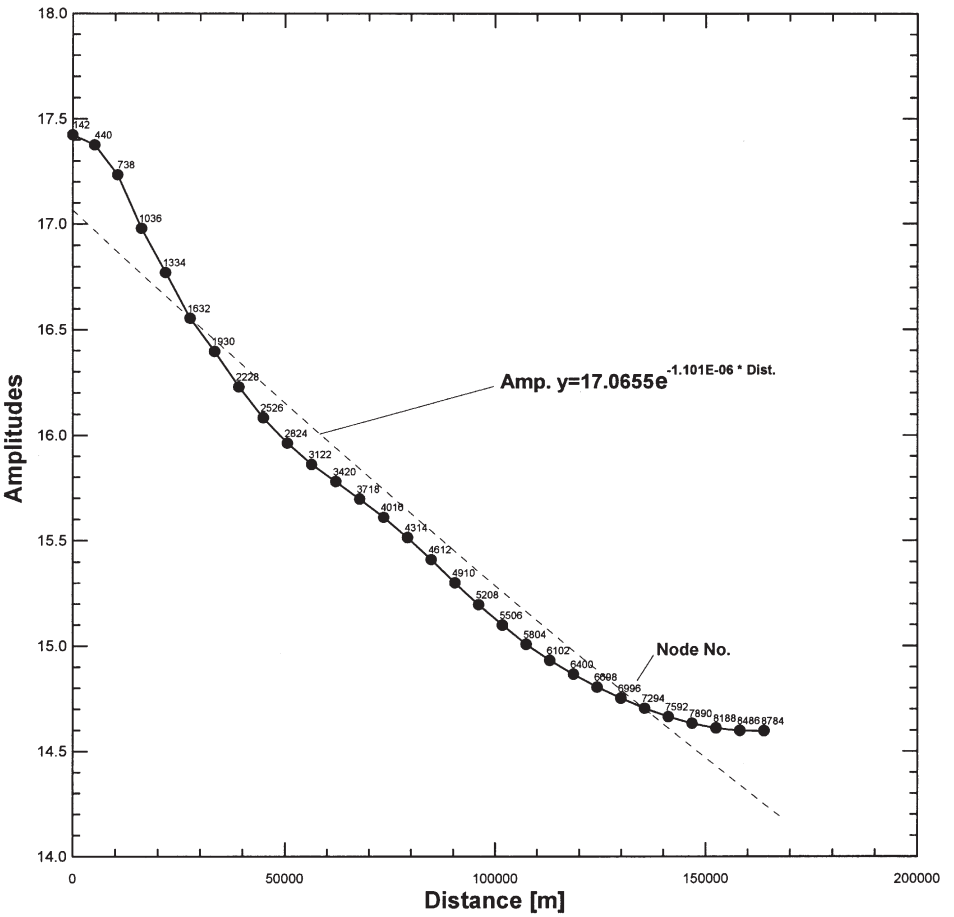

Fig. 9. Numerical amplitude distribution at a selected cross-section from coasts of China to Taichung, Taiwan.

comparisons, partially standing waves can also be observed along the western coast of Taiwan. In addition, the figures also demonstrate that the configurations of partially standing waves are in good agreement with waves trapped with even mode predicted by Mei (1983), for the case of n=2 (refer to Fig. 5). Similar discrepancies between numerical results and field measurements as of M_2 are also observed along the northern stations.

In addition to semidiurnal calculations, computations of diurnal constituent K_1 are also implemented. The corresponding numerical co-range and equi-phase charts with the comparisons are shown in Fig. 13. From the equi-phase chart, Fig. 13(b), it is noted that tidal waves propagate in the direction from north to south and also behave similarly to Poincare waves, whilst partially standing waves are no longer observed. This fact implies that diurnal tidal constituents cannot excite the anomalous amplifi-

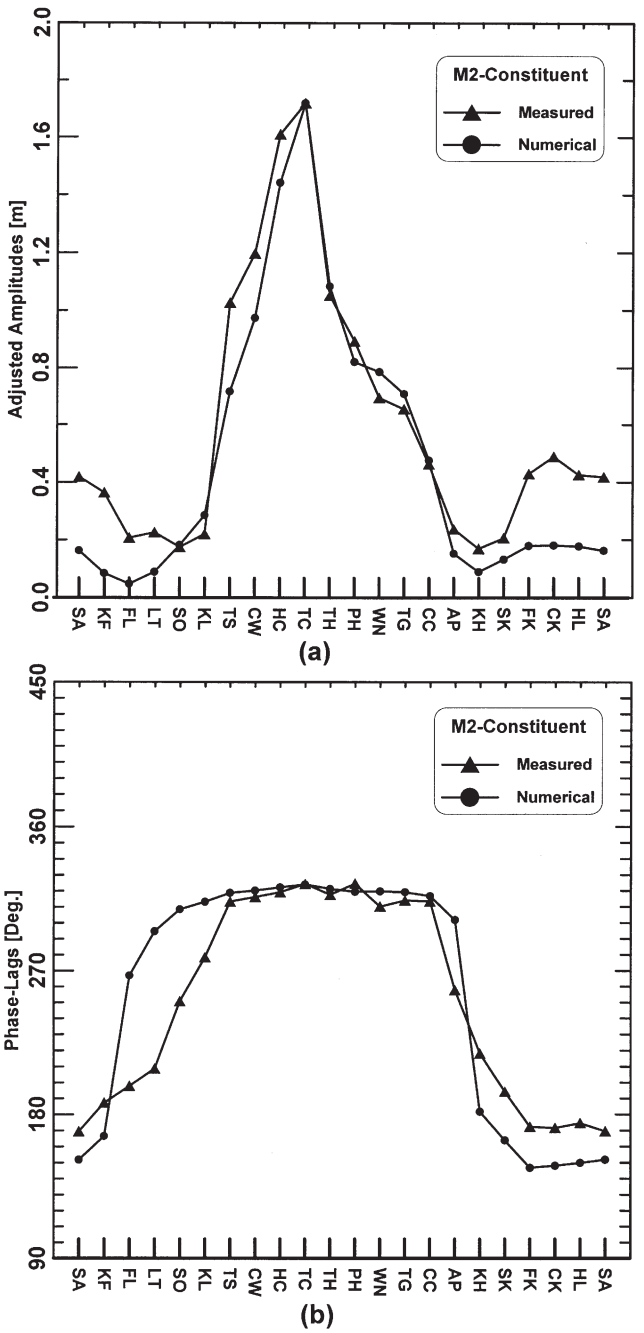

Fig. 10. Comparisons of adjusted amplitudes (a) and of phase-lags (b) of the M_2 constituent with incident angle of 180°.

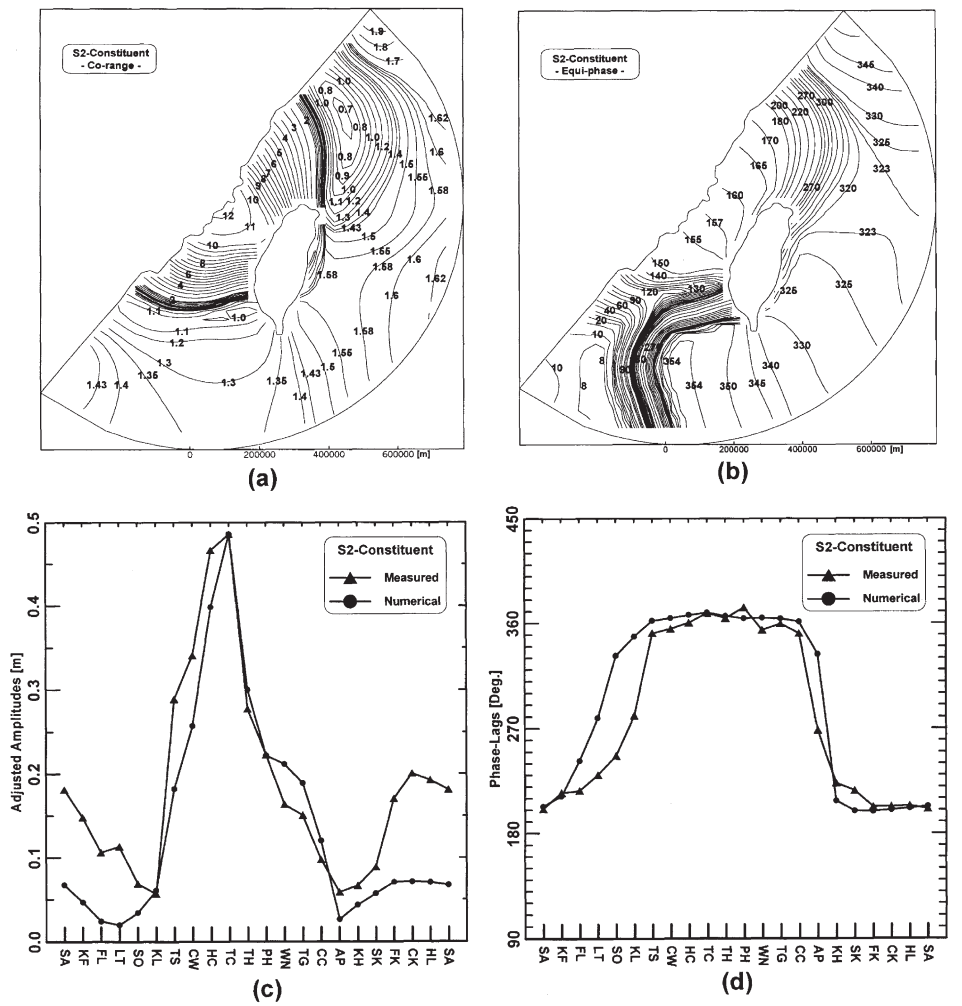

Fig. 11. Numerical co-range (a) and equi-phase (b) charts of the S_2 constituent with comparisons of adjusted amplitudes (c) and of phase-lags (d) with incident angle of 180°.

cation of tides along the western coast of Taiwan. However, large discrepancies in comparing the distribution of phase-lag are observed. The discrepancy may also result from negligence of the Coriolis force. To clarify this speculation, numerical modeling including Coriolis effects is currently underway.

From viewpoints of wave resonance, response curves of amplitude for different tidal periods at representative stations: FL, KL, TC, KH, SK, CK, and HL, around the coasts of Taiwan are shown in Fig. 14. It is noted that when the characteristic periods of semidiurnal constituents approach 13.2 hours with unit incident amplitude, maximum response of amplitude at station TC will appear and approach 22.09 (10.72 for S_2, 14.60 for M_2, 17.49 for N_2, 20.53 for O_2, and 21.19 for $2NS_2$). As to the

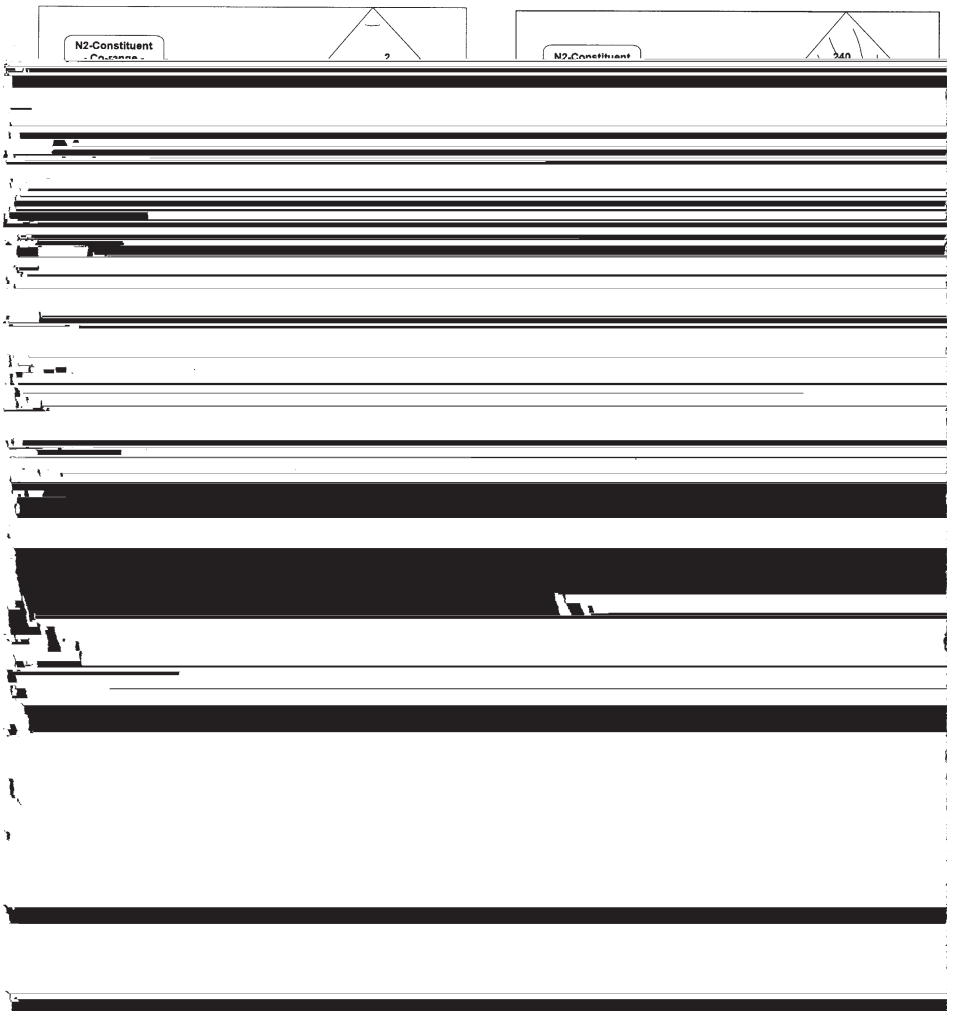

Fig. 12. Numerical co-range (a) and equi-phase (b) charts of the N_2 constituent with comparisons of adjusted amplitudes (c) and of phase-lags (d) with incident angle of 180°.

amplification factors of station TC relative to KL, the computational ratios are 8.03 for S_2, 6.03 for M_2, and 5.27 for N_2. These are in good agreement with measured data that are 8.68 for S_2, 7.85 for M_2, and 5.29 for N_2. For diurnal constituents with characteristic periods approximate to 24 hours, the response factors along the coasts of Taiwan are roughly equal to two, which is mainly induced by shoaling.

From Fig. 14, it is noted that the amplification factor of the central western station, TC, is more significant than those (SK, CK, HL and FL) along the eastern coast. Particularly, even for a tidal resonant period of 13 hours, amplification factors of eastern stations are found approximately equal to unity. This fact justifies furthermore